Focused Ion Beam and Nanomechanical Tests for High Resolution Surface Characterisation: New Resources for Platinum Group Metals Testing

Use of two high resolution techniques allows process optimisation and prediction of in-service behaviour

http://dx.doi.org/10.1595/147106714X675768 http://www.platinummetalsreview.com/

By Marco Sebastiani and Marco Renzelli

University of Rome "Roma Tre" Engineering Department, Via della Vasca Navale 79, 00146 Rome, Italy

Paolo Battaini

8853 SpA Via Pitagora 11, I-20016 Pero, Milano, Italy

Edoardo Bemporad*

University of Rome "Roma Tre" Engineering Department, Via della Vasca Navale 79, 00146 Rome, Italy

*Email: edoardo.bemporad@uniroma3.it

Recently, the increasing importance and scope of nanotechnology has extended the need for high resolution characterisation tools beyond their traditional domains. As a consequence, advanced high-resolution tools at the nanoscale are now increasingly used in research and development (R&D) activities, offering the chance for a better understanding of submicron feature size dependence. This paper gives an overview of the synergic application of two high resolution techniques on the platinum group metals (pgms): focused ion beam (FIB) coupled with electron beam imaging, milling and deposition techniques; and nanoindentation testing. After a brief description of both techniques (architecture, probe-sample interaction basics and operation modes), the effectiveness of this combined approach is demonstrated for microstructural and nanomechanical investigations on very small samples. The advantages are low cost, fast and site-specific sample preparation for transition electron microscopy (TEM) analysis; study of the mechanical hardening effect on microstructure and hardness profile at the micron scale; failure analysis; and understanding of plasticity and elasticity behaviour. Two specific case studies related to a platinum-copper alloy for jewellery use and a platinum-rhodium alloy for sensor manufacturing are presented and discussed.

1. Introduction

The structural characterisation of engineered surfaces is of increasing importance due to the growing application of surface modification processes and coating techniques, which are usually applied to improve either mechanical or functional surface performance. Some examples include surface hardness, load bearing capacity, impact bearing capacity, wear resistance, specific surface area (related to surface free energy and chemical reactivity),

electrical resistivity, thermal conductivity and 'smart' optical properties (1).

The development of nanostructured materials and the increasing use of nanosystems and nanostructures make the use of advanced procedures for nanoscale mechanical characterisation necessary to understand chemical and physical phenomena at this scale (2). The in-service macroscale mechanical behaviour of micro- and nanocrystalline metals (for example, their fracture and plastic deformation behaviour) is strictly related to the complex interactions between the different micro- and nanostructural features (for example dislocation sources, grain boundaries and nanoscale porosity). These latter aspects are particularly critical in the advanced metallurgy of pgms alloys, where the actual role of phase transitions, the microstructural evolution of interfaces during processing and the correlation with their mechanical properties are not yet completely understood.

The in-service performance of such materials is dependent on the evolution of nano- and microstructural features during processing, including development of nanodispersed phases, grain growth, evolution and composition of grain boundaries, dislocation density and distribution. Therefore an understanding of the correlation between the micro- or nanostructure and the mechanical properties of a material is critical for the development of new and improved materials. High resolution microscopy analysis together with nanomechanical characterisation are powerful tools that can allow such understanding.

The present paper gives an overview of the synergic use of two high resolution techniques, which are expected to be established as enabling technologies for improving the current understanding of the correlations between process, microstructure, properties and performance for precious metal alloys. These are:

- FIB coupled with electron beam for imaging, milling and deposition (referred to as 'dualbeam' (3–5))
- Nanoindentation (6–12) for hardness measurement with a very low load.

1.1 Advantages of the Techniques

A key advantage of these two techniques (FIB/SEM and nanoindentation) for high-technology manufacturing is that both are very site-specific and virtually artefact free in measuring as well as in imaging or shaping samples in order to expose the region of interest. Moreover, some analysis on cross-sections and even TEM lamellae extraction are virtually nondestructive, as the sample size required is just a few cubic microns.

In this paper, two examples are outlined to show how the combined use of nanomechanical testing and high resolution microscopy can help gain understanding of the processing mechanisms and in-service behaviour of components. In particular:

- Cross-section cut-and-view for rapid microstructural investigation (grain size and inclusions) on very small samples without any sample preparation or preprocessing (dualbeam)
- Low cost, fast and site-specific sample preparation for TEM analysis (dualbeam)
- Deformation mechanisms at the nanoscale (dualbeam and nanoindentation)
- Mechanical hardening effect on microstructure and hardness profile at the micron scale (dualbeam and nanoindentation)
- Separate measurement of elastic modulus, apparent hardness, true hardness, plasticity and hardening behaviour (nanoindentation).

The article will focus on two case studies, explaining the importance of the combined use of dualbeam and nanomechanical testing for the correct evaluation of mechanical and functional performances of nanostructured systems in the pgms:

- Order hardening of platinum-5 wt% copper alloys: microstructural and nanomechanical characterisation for this alloy used in jewellery;
- Influence of process history on microstructure and mechanical properties of platinum-rhodium alloys, used in thermocouples.

In both cases, it will be demonstrated that nanoindentation testing can give valuable information on the microstructural changes due to phase transition and intragrain microstructure. In addition, the combined use of FIB/scanning electron microscope (SEM) and TEM techniques could help to understand how and why microstructural changes due to heat and/or mechanical treatments affect the mechanical behaviour of samples.

1.2 Brief Introduction to Focused Ion Beam (FIB) Techniques

FIB technology was first introduced in the 1980s in the semiconductor industry. FIB instruments derive their design from the SEM. However while SEM instruments use electrons that are accelerated and focused on a surface, FIB uses ions (usually gallium). The image is derived from secondary electrons resulting from

the particle irradiation. The use of ions means that it is not only possible to image the surface but also to mill it, using sputtering phenomena to remove material. From an engineering point of view, the two instruments, albeit similar in concept, are different in construction: the high mass of the ions requires electrostatic lenses, instead of electromagnetic lenses as used in SEM (3–5).

The new generation of FIB equipment is equipped with both an ion beam column and an electron beam column (SEM), providing imaging of the ion beam milling process. In this case the instrument is called a dualbeam microscope (**Figure 1(a)**). It can be seen from **Figure 1(a)** that the instrument can use the electron and ion columns at the same time; considering that the resolution of the FIB is 5 nm, it is possible to mill the surface in real time with nanometre resolution, working it with ions and observing it with electrons, as in **Figure 1(b)**. In dualbeam with *in situ* SEM three dimensional tomography can be obtained by the slice-and-view process (3–5). An additional feature of FIB is the capability to deposit thin films (for example, made from Pt or carbon) by ion- or electron-assisted chemical vapour deposition (CVD), as shown in **Figure 1(b)**.

FIB milling can be performed on hard, soft and biological materials with minimal artefacts (3–5). Some Ga atom implantation and amorphous layers will typically be observed but these artefacts can be limited to a thickness of a few nanometres by careful selection of the milling parameters (mainly current and voltage). FIB systems use a focused beam of Ga^+ ions at low beam currents (of the order of pA) for imaging and at high beam currents (of the order of nA) for site-specific milling.

FIB techniques can be also used for TEM lamella preparation: a finished electron transparent portion of the sample (usually 5 μm × 20 μm) is obtained by FIB milling (performed at 30 kV by using a decreasing sequence of ion milling currents, from 9 nA down to 0.28 nA for the final polishing) and then carried by a micromanipulator on a sample holder to be inserted into the TEM microscope: this procedure at present represents the best site-specific and artefact-free TEM sample preparation methodology. **Figure 2** illustrates how a dualbeam can be used to prepare site specific thin sections for high resolution TEM imaging and analysis.

1.3 Brief Introduction to Nanoindentation Testing

Nanoindentation testing (6) has been widely adopted in the last two decades for the surface mechanical characterisation of bulk materials and coatings. The method involves the controlled penetration of a diamond indenter of known shape into the material. Usually, a three-sided pyramidal indenter (Berkovich) is used in conventional nanoindentation. By measuring the load and displacement during the loading and unloading parts of the test, hardness (i.e. resistance to plastic deformation) and elastic modulus can be calculated (6, 7). In this way, a very accurate characterisation of the elastic and plastic properties at a material's surface can be achieved, with a depth resolution and a lateral spatial resolution of the order of a few nanometres.

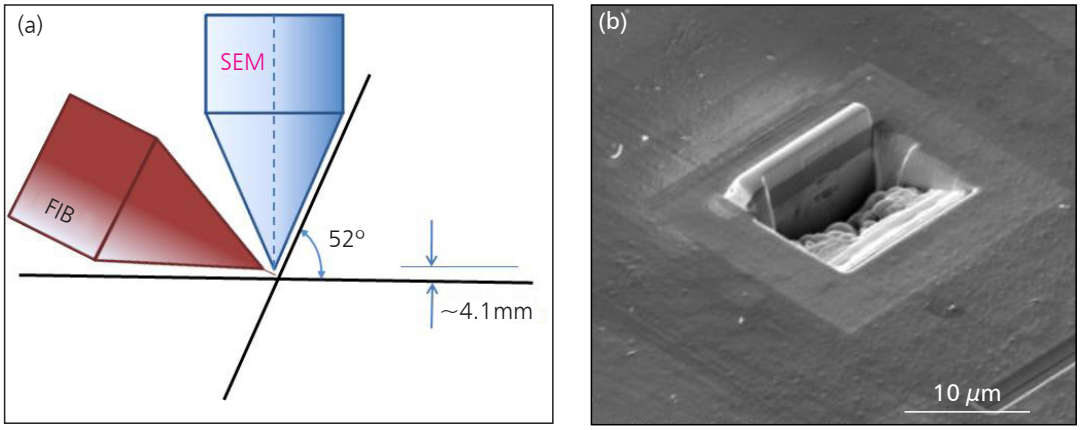

Fig. 1. (a) Schematic of dualbeam FIB/SEM equipment; (b) an example of a cross-section by FIB. A thin layer of Pt is deposited before ion milling

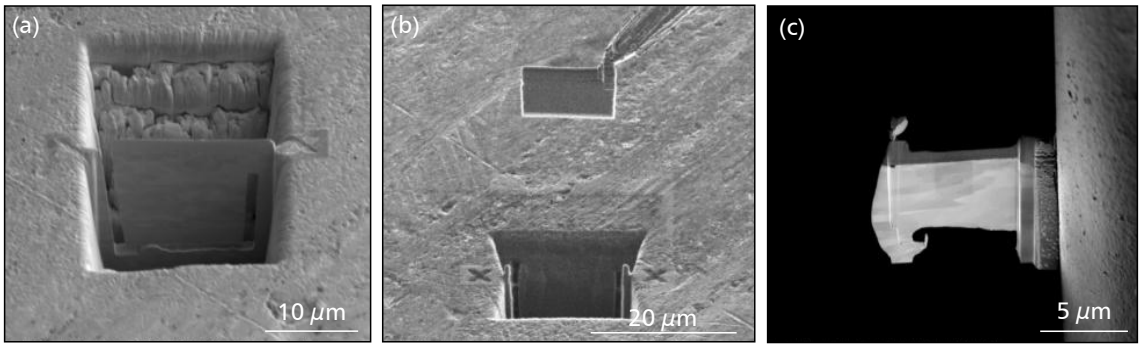

Fig. 2. Sequence for TEM lamella preparation by FIB techniques for a Pt-Cu alloy: (a) FIB milling of a thick lamella and cutting section (~300 nm, milled at 0.92 nA); (b) lift-out of the lamella by the micromanipulator; (c) welding of the lamella on the TEM sample holder and final thinning to electron transparency (~80 nm, at a current of 0.28 nA)

During a basic indentation test an ideally rigid indenter of known geometry is pressed against the sample surface up to a controlled maximum load, following a controlled loading (or displacement) rate. When the indenter is driven into the material, both elastic and plastic deformation processes occur, producing a hardness impression that conforms to the shape of the indenter to a certain contact depth, h_c (**Figure 3(a)**).

The hardness H is easily obtained as a function of load (or penetration depth) by the following equation:

$$H = \frac{P}{A_c} \qquad \text{(i)}$$

where P is the maximum load and A_c is the indenter projected contact area, which is given as a polynomial function of the contact depth, h_c, for a Berkovich indenter:

$$A_c = a_0 h_c^{\,2} + a_1 h_c + a_2 h_c^{\,1/4} + a_3 h_c^{\,1/8} + \ldots \qquad \text{(ii)}$$

The contact depth is defined as follows (see also **Figure 3(a)**):

$$h_c = h - \varepsilon \cdot \frac{P}{S} \qquad \text{(iii)}$$

The coefficient ε can range between 0.72 and 1; a value of 0.75 is usually adopted for the Berkovich indenter.

The contact area expressed in Equation (ii) is evaluated by calibration on a certified fused silica reference sample, performed before and after each series of tests. As the indenter is removed from the surface, a purely elastic recovery phenomenon occurs, thus giving a measurable unloading elastic contact

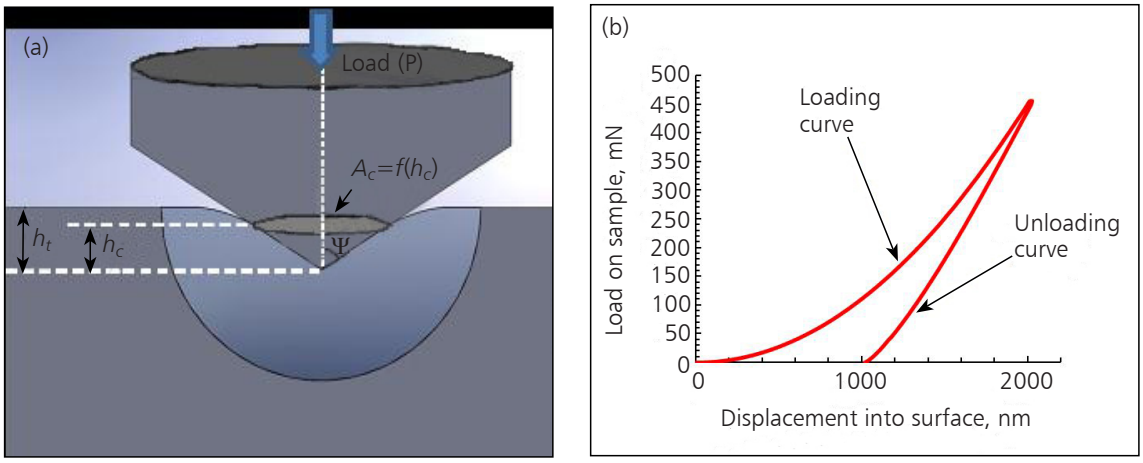

Fig. 3. (a) Contact geometry usually adopted in modelling sharp indentation testing. The equivalent cone angle ψ is equal to 70.3° for the Berkovich and Vickers indenters; (b) an example of a load-displacement curve for an amorphous fused silica reference sample

stiffness, which can be analytically correlated to both the material's and the indenter's elastic properties by the use of the Sneddon solution for the contact on an axisymmetric elastic body on a flat surface (6):

$$E_r = \frac{\sqrt{\pi}}{2\beta} \cdot \frac{S}{\sqrt{A}} \qquad \text{(iv)}$$

$S=dP/dh$ is the elastic contact stiffness which is evaluated, after fitting the upper portion (usually 50%) of the unloading curve to a power-law relation (Oliver-Pharr method (6)), as the slope of the unloading curve at maximum load P_{max}.

E_r is the reduced modulus (which takes into account both the elastic deformation of sample and indenter), given by:

$$\frac{1}{E^*} = \frac{\left(1-\nu_s^2\right)}{E_s} + \frac{\left(1-\nu_i^2\right)}{E_i} \qquad \text{(v)}$$

where E_i and ν_i are, respectively, the Young's modulus and the Poisson ratio of the indenter. β is a numerical correcting factor equal to 1.034 for a Berkovich indenter, which is introduced to correct for the lack of symmetry of the indenter with respect to the ideal conical shape. As recently reviewed by Oliver and Pharr (6), values in the range of $1.0226 \leq \beta \leq 1.085$ can be found in the literature; in the present work the value of 1.000 is adopted, as suggested by the ISO 14577-1-2 standard.

Equations (i)–(v) give a short synthesis of the Oliver-Pharr method (see also **Figure 4**), which is conventionally adopted for the analysis of hardness and elastic modulus from a generic nanoindentation test.

An interesting modification of the conventional nanoindentation is the so called 'continuous stiffness measurement' (CSM) method. In the CSM method (7), the contact stiffness S is dynamically measured during indentation and continuous hardness/depth and modulus/depth curves are obtained using Equations (i)–(v).

Apart from the most conventional analysis, nanoindentation testing has been used for the evaluation of several other surface mechanical properties, such as yield strength and strain hardening behaviour of metals (7, 8), damping and internal friction in polymers (i.e. storage and loss modulus), activation energy and stress exponent for creep (8), fracture toughness of bulk ceramics and coatings (9), adhesion of thin films and work of adhesion (11), scale effects in mechanical behaviour of small scale specimens (11) and residual stress (12, 13).

In the case of metals, significant dependence of the measured hardness on the applied load is usually observed, even if a self-similar indenter is used for testing (for example, a pyramidal indenter). This experimental evidence, which is usually referred to as 'indentation size effect' (ISE), is not only due to the effects of surface preparation (i.e. surface hardening) and/or indenter tip blunting (i.e. not perfectly sharp indenters), but also to a real 'material scale-dependent plasticity', that has been related to subsurface modifications of the dislocation density across the plastically deformed volume which is created during indentation.

The most diffused model to understand ISE was proposed by Nix and Gao (10). The model is based on a simple concept, that 'geometrically necessary dislocations' (GNDs) must be created in the plastically deformed volume (beneath the indenter) to accommodate the deformed material from the surface. The GNDs exist in addition to the other statistically stored dislocations (SSDs), which are usually present in any polycrystalline metal. The additional amount of GNDs gives rise to an additional hardening effect, which is higher as the size of indentation decreases, thus explaining the observation of increasing hardness with decreasing applied load.

Starting from this idea and assuming a conical rigid indenter, Nix and Gao came out with a simple equation describing the variation of hardness as a function of the penetration depth during indentation:

$$H = H_0\sqrt{1+\frac{h^*}{h}} \qquad \text{(vi)}$$

where H_0 is the macroscale hardness and h^* is a characteristic length scale, which depends both on the material's properties and the indenter geometry.

2. Case Study 1: Microstructural and Nanomechanical Characterisation of Pt-5%Cu Order Hardened Alloys

Pt-5 wt% Cu alloys are used in jewellery mainly because the addition of Cu significantly improves the mechanical properties compared to pure Pt, particularly its resistance to plastic deformation (i.e. yield strength and hardness); it is also known that heat treatment of Pt-5 wt% Cu alloys can result in a further increase of indentation hardness (often

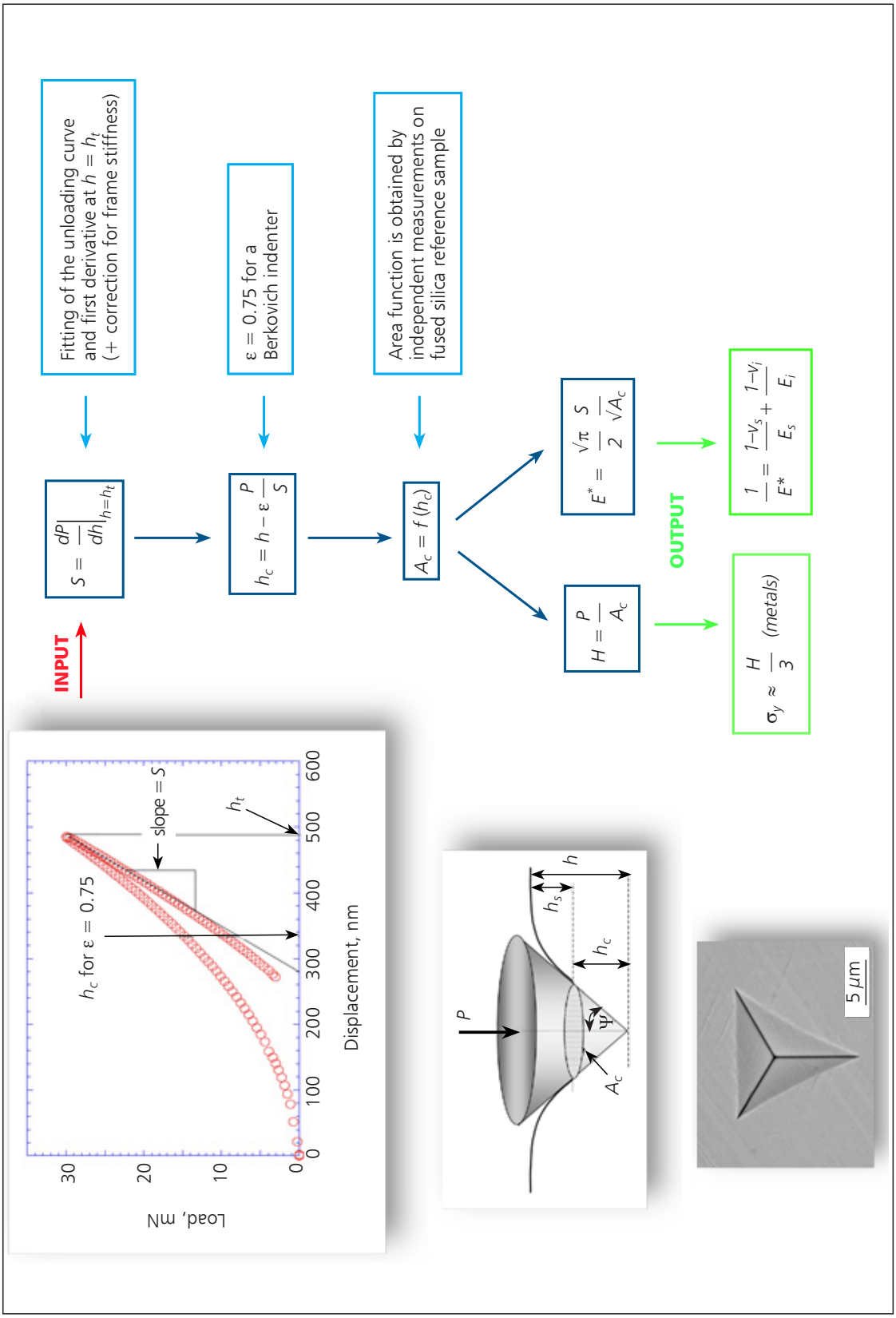

Fig. 4. Oliver and Pharr method for hardness and elastic modulus evaluation by nanoindentation (7)

measured by Vickers microhardness testing) (14). This phenomenon is related to the fact that the Pt-Cu binary system forms an ordered structure (described by the CuPt7 model) from the disordered face-centred cubic (fcc) solid solution, in the composition range 12–25 at% Cu (14).

It has also been previously reported that the order-disorder transition can be strongly enhanced by inducing a certain quantity of microstructural defects in the structure, for example, by quenching or by plastic deformation (14).

A recent paper (15) reports a study of the order-disorder transition in Pt-5 wt% Cu alloys using TEM-selected area electron diffraction (SAED) probing, showing that initially quenched specimens were characterised by relatively larger ordered domains after heat treatment and by a lower increase of Vickers hardness in comparison with cold plastically deformed samples. Nevertheless, a deeper analysis of the influence of the mechanical hardening process on the microstructural and structural characteristics of order-disorder transition is still required, in order to discover the optimal cold working process in terms of induced plastic strain and induced modification of hardness and of hardening coefficient, which can guarantee the maximum increase of hardness after heat treatment. Furthermore, there is still a strong necessity for the development of more reliable and accurate procedures for the technological assessment of phase transitions after heat treatment.

In this section, an innovative procedure for the mechanical and microstructural characterisation of Pt-Cu order hardened alloys is presented, essentially based on the combined use of micro- and nanoindentation testing and ISE modelling, dualbeam and TEM techniques. It is shown that the correct modelling of micro- and nanoindentation hardness results coupled with high resolution dualbeam and TEM observations can give deeper information on the actual influence of the preliminary cold working process on the order hardening transition.

2.1 Experimental Details

One as cast Pt-5 wt% Cu ingot was subjected to homogenisation at 1000ºC for 15 h and then plastically deformed by uniaxial compression (milled) with a thickness reduction of 75%. From the milled plate two samples were cut. One of these two samples was heat treated at 290ºC for 3 h and finally cooled in air. The hardness of both samples was studied by nanoindentation testing by means of a Berkovich diamond indenter, using an Agilent G200 Nano Indenter, in a CSM mode under a constant strain rate of 0.05 s^{-1} and a maximum penetration depth of 2000 nm (other test and fitting parameters were chosen according to ISO 14577-1-2 standards) (18). Cross-section SEM-field emission guns (SEM-FEG) microstructural observation and TEM-SAED analyses were performed after FIB sample preparation in a dualbeam (FEI Helios Nanolab 600).

Cross-sections were obtained by FIB milling after a preliminary *in situ* Pt deposition to protect the surface layers during ion milling; the sectioning process consisted of a preliminary high ion current milling (9 nA) followed by cleaning the section (0.9 nA) until the desired section was obtained. Microstructural observation was performed using both the ion probe (maximum microstructural contrast) and the electron probe (maximum morphological contrast), secondary electrons were detected in both cases. The dualbeam technique was also used to extract electron transparent foils for TEM (Philips CM 120, LaB6 analytical). TEM analyses consisted of bright field high magnification observation followed by SAED, performed both at the surface of the TEM foil and at its centre.

2.2 Results and Discussion

The results of the nanoindentation testing are reported in **Figure 5** and summarised in **Table I**. The nanohardness profiles presented in **Figure 5** clearly confirm that the hardness is significantly increased after heat treatment. Furthermore, in this case, the presence of a surface hardened layer is observed for penetration depths lower than 500 nm. Nanoindentation testing allows a more detailed analysis of this effect to be performed: it is very important to note that the hardness profiles for both samples have a very similar shape, i.e. a very similar skin effect is observed in both cases.

This observation suggests that the microstructure derived from the cold working process (which likely involves the formation of a surface hardened layer) is completely maintained after heat treatment, because the same hardness gradient is observed in both cases. This also means that neither recrystallisation nor changes of grain size occurred during the heat treatment at 290ºC, suggesting that the order-disorder phase transition is realised at a subgrain level with no significant modification of dislocation density.

Another relevant observation comes from SEM-FEG imaging of the nanoindentation marks. **Figure 6** shows the rounded shape of the indent lateral profile.

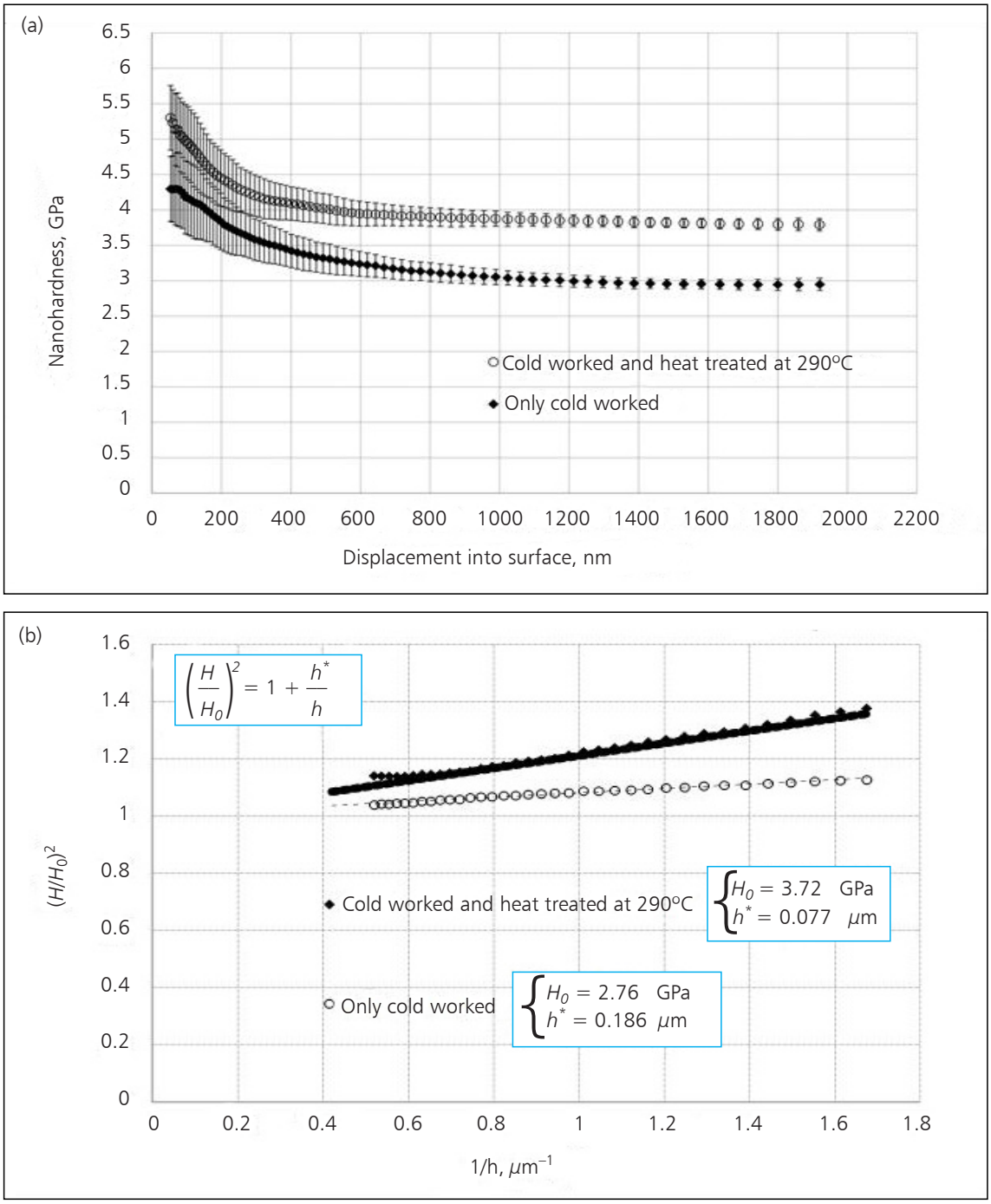

Fig. 5. (a) Nanoindentation hardness depth for both Pt-Cu samples under investigation; (b) analysis of hardness data through the Nix-Gao ISE model. Hardness is confirmed to be higher for the heat treated sample

From **Figure 6(b)** it can be clearly seen that for the heat treated sample there was a higher amount of piling up at the edge of indentation. This suggests that the heat treatment may have influenced not only hardness, but also the hardening coefficient of the sample. As reported earlier (8), a different hardening coefficient usually involves a different amount of piling-up during indentation.

Table I

Summary of Results for the Micro- and Nanomechanical Characterisation of Platinum-5 wt% Copper Samples

	Hardness[a], GPa	Modulus[a], GPa	Nix-Gao parameters (Equation (vi)) (H_0; h^*), GPa; μm
Cold worked sample	3.08 ± 0.11	205.1 ± 4.7	2.76; 0.186
Cold worked and heat treated sample	3.88 ± 0.21	215.2 ± 7.1	3.72; 0.077

[a] *Average in the penetration depth range of 300–900 nm*

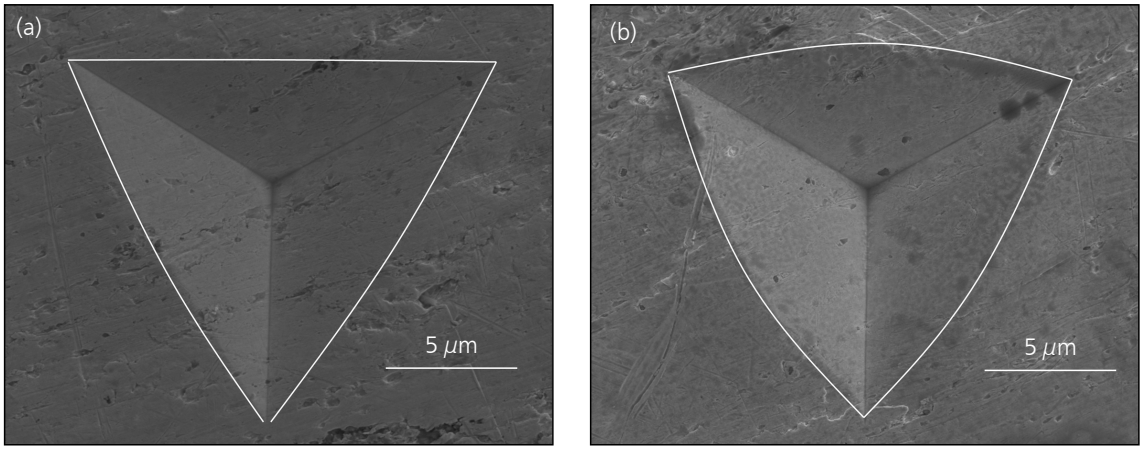

Fig. 6. Dualbeam (SEM column) micrographs on Berkovich nanoindentation marks for: (a) cold worked sample; (b) cold worked and heat treated sample. A higher amount of piling up is observed in case of the heat treated sample, thus suggesting that order hardening also involves a modification of the hardening coefficient

This observation is confirmed by an analysis of the hardness data using the Nix-Gao ISE model (10), where a significantly different value of the h^* parameter is found (see **Table I** and **Figure 5(b)**), thus suggesting that the two samples may have a different hardening coefficient. This leads to a very important conclusion: the hardening behaviour (not only hardness) of the heat treated sample is modified, which can have a significant effect on workability and on service performance of materials heat treated in such a way.

The results of the indentation modulus profile are reported in **Figure 7**, where elastic modulus is shown to be constant with penetration depth and does not depend on sample microstructure (as expected). The elastic modulus seems to be ~5% higher for the heat treated sample, however this is not considered statistically significant. This difference is likely due to the observed pile-up during indentation. As widely reported in the literature, piling up always involves an over-estimation of the measured elastic modulus, due to incorrect evaluation of the real contact area by the Oliver-Pharr method (7). The observed difference in the elastic modulus is therefore likely not to be a real effect, thus suggesting that modulus does not change significantly after the heat treatment (as expected).

In both **Figures 8** and **9**, the left column refers to the cold worked sample, while the right column refers to the cold worked and heat treated sample. Dualbeam characterisation analysis clearly shows that the microstructure and microscale morphology of both samples are very similar. In both cases, a strongly oriented (biaxial) grain structure is observed, which is likely to be a consequence of the cold forming process. These results confirm that the microstructure of the sample is not modified by the

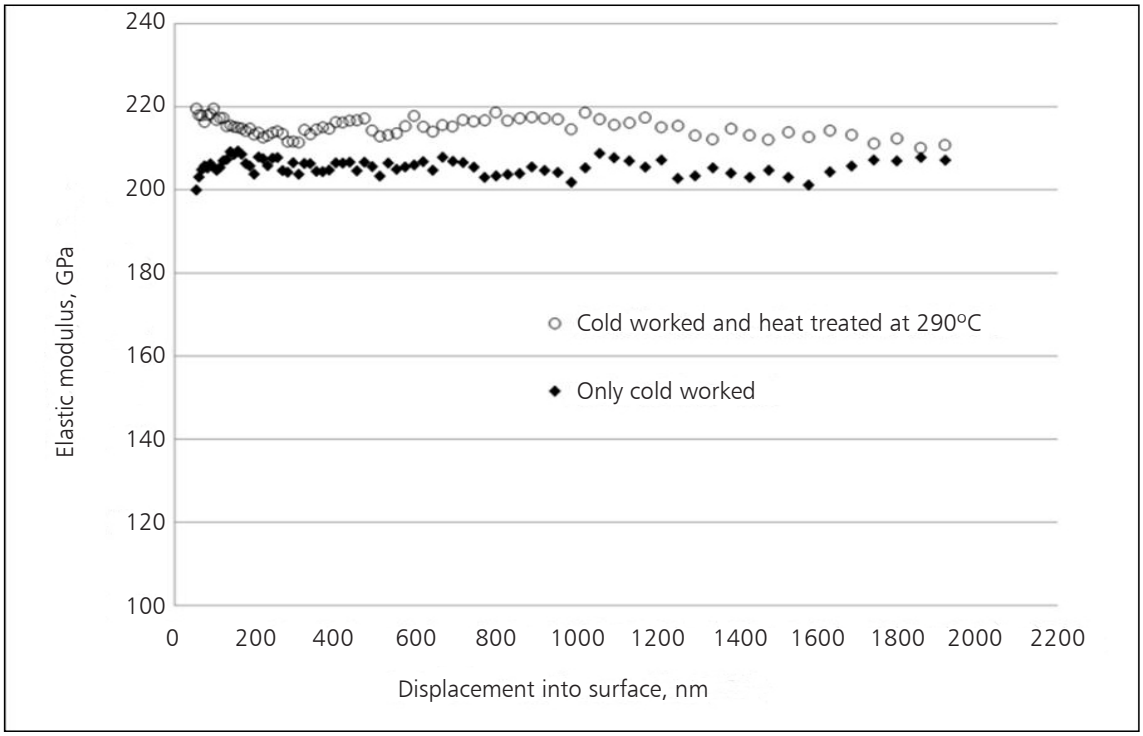

Fig. 7. Elastic modulus as measured by nanoindentation testing for both samples

heat treatment and that the order-disorder transition is likely to happen at a subgrain level. A similar result can be achieved by a careful analysis of the nanoindentation hardness profile.

The results of TEM-SAED analysis on dualbeam prepared thin foils are reported in **Figure 9**. **Figures 9(a)** and **9(e)** show detail of the grain structure at the sample surfaces. It is clear that the grain structure has been maintained almost identically after heat treatment and that the dislocation density is similar in both cases, confirming the results obtained by nanoindentation and dualbeam cross-section observation. In addition, a very thin surface hardened layer (characterised by a finer grain size) is clearly shown in **Figures 9(b)** and **9(f)**. **Figures 9(c)–(g)** show details of the intragrain morphology, which are significantly different for the two samples. In the case of the heat treated sample the ordered domains are clearly visible confirming that the phase transition happens at a subgrain level.

In addition, a complete change of dislocation distribution is evident in the ordered domain, suggesting that dislocations (or generally speaking, all defects coming from plastic deformation) can be considered the main nucleation sites for the phase transition. This explains why the order-disorder transition is usually observed only for seriously plastically deformed samples and not for quenched or as-cast samples.

3. Case Study 2: Influence of Process History on Microstructure and Mechanical Properties of Platinum-Rhodium Alloys

Alloys of Pt and Rh (19, 20) are widely used in many industrial sectors, due to their high strength compared to pure Pt, good workability and very good corrosion resistance even at high temperature. Examples from industry include thermocouples for high-temperature measurement, clean and inert heating elements in experimental high-temperature furnaces, components in the manufacture of glasses, catalyst gauzes and laboratory equipment (21–24). The use of Pt-Rh alloys has been increasing due to the fact that Rh dissolves in all proportions in Pt, thus forming a substitutional solid solution which usually involves an increase of hardness with no significant loss of workability.

However, there are still controversial results in the literature on the actual phase evolution of Pt-Rh systems at temperature below 1033 K. Some authors have proposed the presence of a miscibility gap below 1033 K (19), which was not confirmed

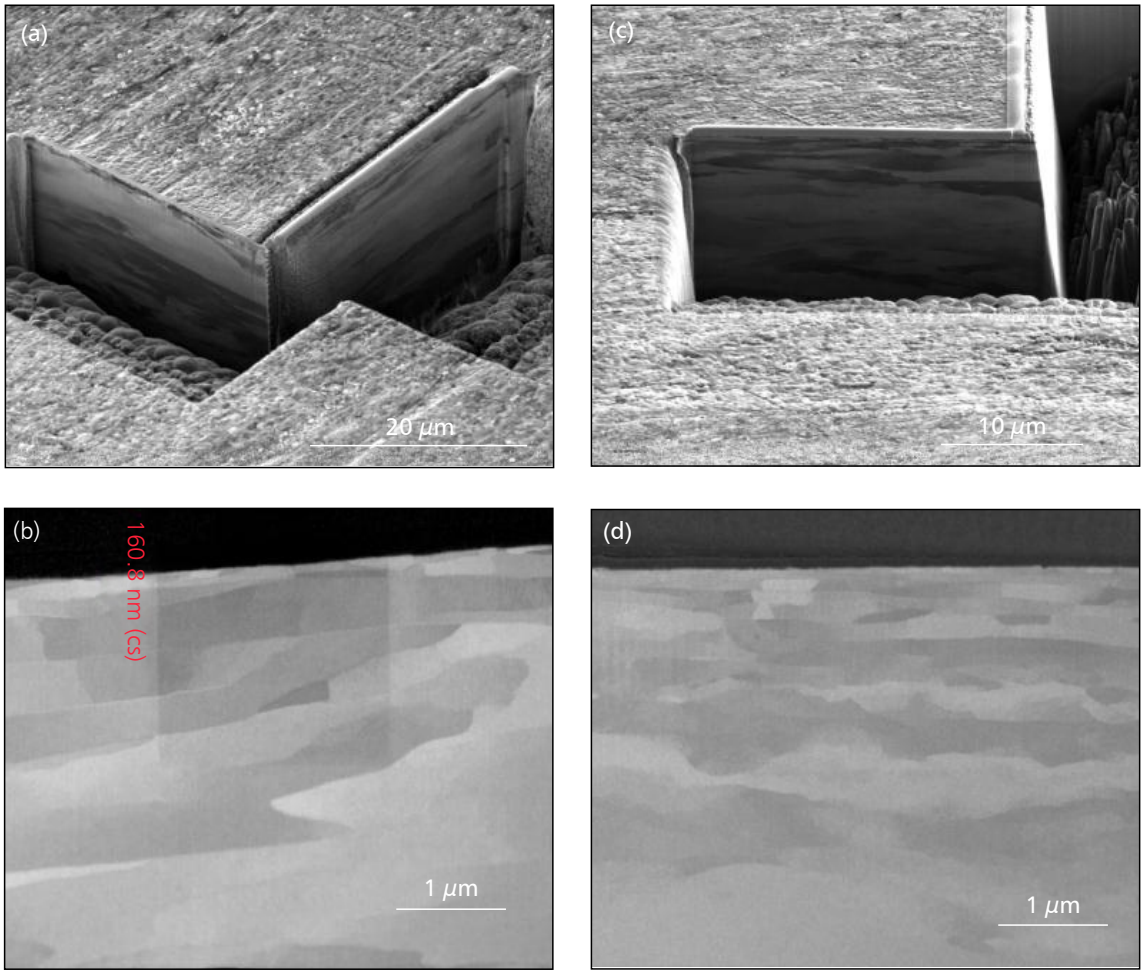

Fig. 8. Dualbeam (FIB and SEM column) analysis of samples: (a) and (b) the cold worked sample; (c) and (d) the cold worked and heat treated sample. It is worth noting that the microstructure obtained after cold working is maintained after heat treatment, including the surface hardened layer

by other similar studies, thus suggesting that further investigations should take place to achieve a better and deeper understanding of the actual microstructural and phase evolution of Pt-Rh systems after heat treatment and cooling to room temperature (20).

Another issue of interest is represented by the observed tendency to oxidation of Rh after heat treatment of Pt-Rh systems, which usually involves a decrease in the indentation hardness of the samples; in the case of industrially produced components (for example, wires) the mechanisms of oxidation behaviour as a function of process parameters have not been completely investigated. These examples suggest that innovative characterisation procedures are strongly needed, with the main objective of finding out the existing correlations between the observed microstructures and the technological performance (for example, hardness) of the components. This data can then be used to optimise the process parameters.

In this work, the usefulness of the above described procedure for the microstructural and nanomechanical characterisation is demonstrated for Pt-10 wt% Rh wires. Two different industrially produced samples (which were expected to be identical) were investigated by high resolution microscopy techniques (dualbeam-TEM) and nanoindentation testing. A correlation between the observed differences in terms of indentation hardness and the actual microstructure is finally presented.

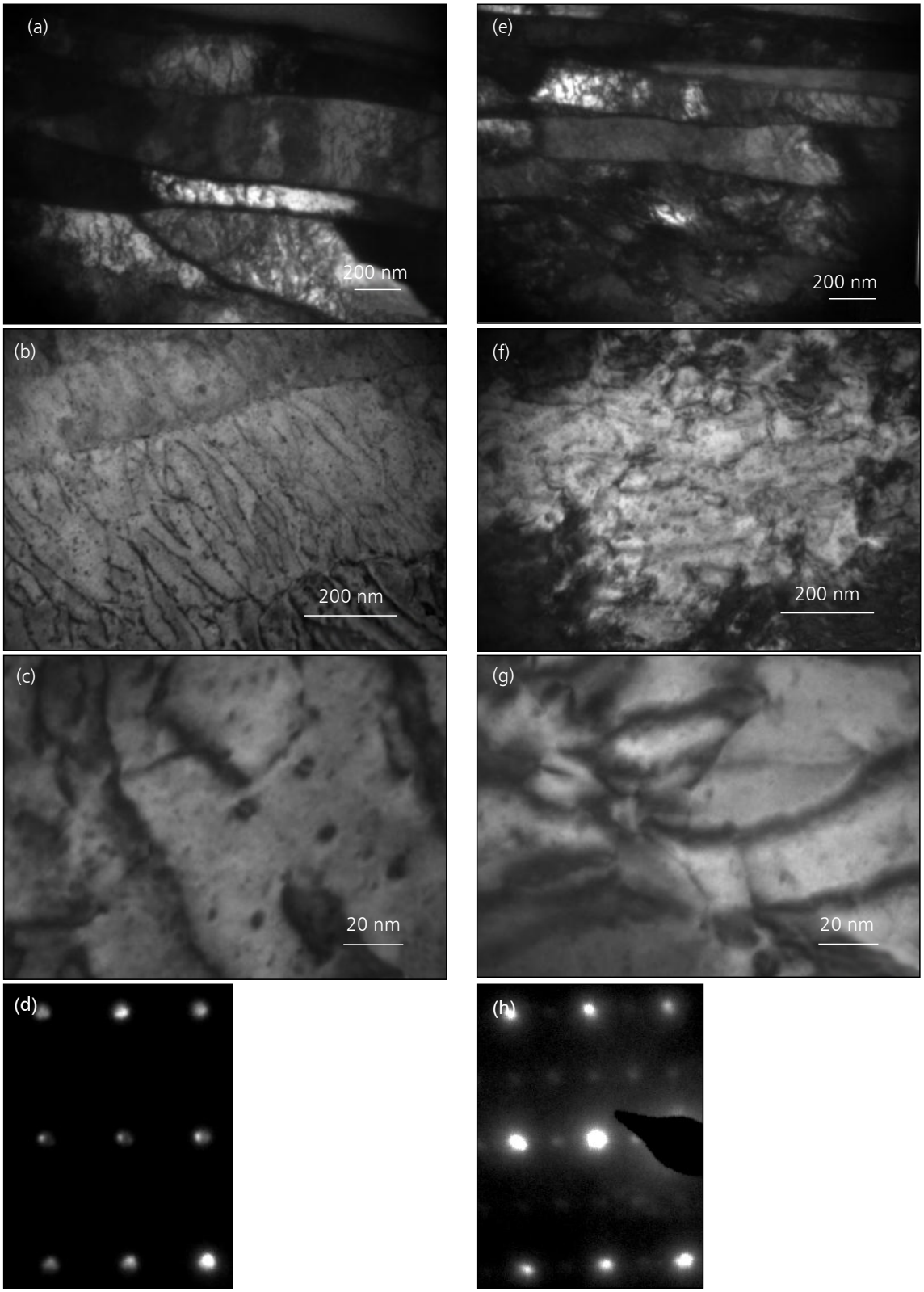

Fig. 9. TEM-SAED analysis on dualbeam prepared thin foils: (a), (b), (c) and (d) cold worked samples; (e), (f), (g) and (h) cold worked and heat treated samples. High dislocation density is observed in both cases. Order hardening is observed at a subgrain level; (d) and (h) SAED patterns clearly show the change of crystal structure after heat treatment

3.1 Experimental Details

Two sets of Pt-10 wt% Rh wires from two different producers, referred to as Sample 1 and Sample 2, were investigated. The samples were nominally produced by the same process, consisting of various stages of drawing and annealing from the initial ingot down to the final section of about 350 μm. Vickers hardness (applied load 100 gf) was preliminarily performed on both samples and a significant difference was observed (as briefly reported in **Figures 11(a)** and **11(b)**). In particular the Vickers hardness was about 15% higher for Sample 2.

Starting from this preliminary result, characterisation activities consisted of dualbeam-TEM microstructural observations and nanoindentation testing. The ion beam was used at a current of 48 pA in the dualbeam microscope to produce physical etching of the microstructure: in this way, the cross-section grain structure of the wires could be investigated by using the ion source and detecting secondary electrons.

A TEM lamella was realised at the external edge of each sample: one grain boundary was included at the centre of each lamella, as reported in **Figure 10**. In this way, all microstructural features influencing the mechanical properties of the wires were able to be investigated (for example, subgrain microstructure, grain boundary oxidation, presence of precipitates at grain boundary or in the matrix and oxygen diffusion from the sample edge).

Nanoindentation testing was used to evaluate the subgrain hardness profile: one line of Berkovich indentation (maximum penetration depth 1 μm, CSM mode, 0.05 s^{-1} constant strain rate) was realised across the section of each wire. The measured hardness profile was then compared to the observed grain structure.

3.2 Results and Discussion

Conventional metallographic observations are shown in **Figure 11**. Dualbeam observation with ion source

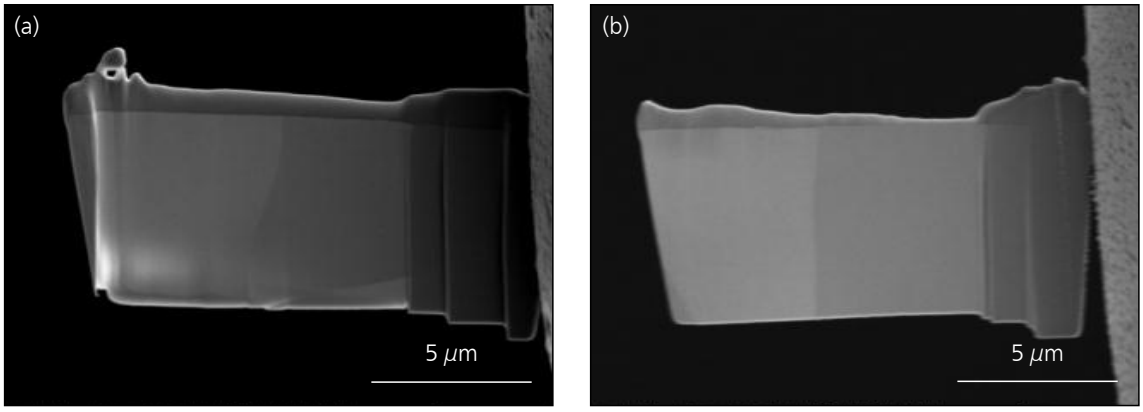

Fig. 10. TEM lamella for: (a) Sample 1; and (b) Sample 2. A grain boundary is clearly visible in both cases

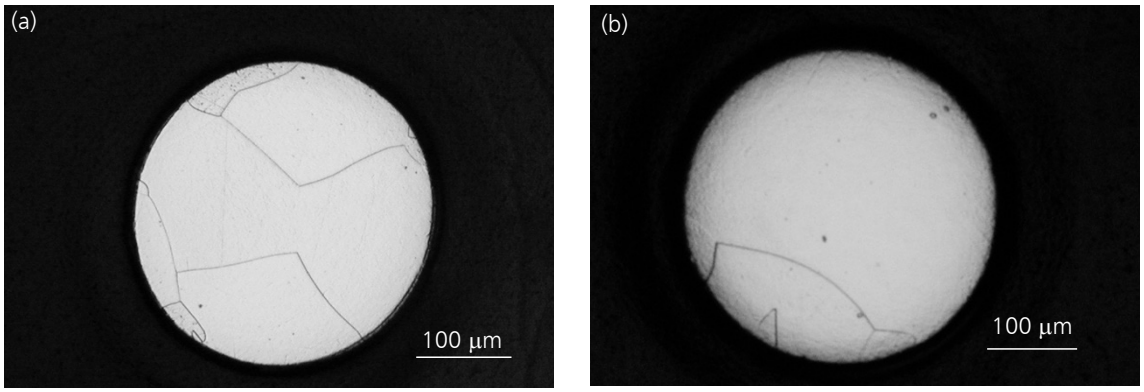

Fig. 11. (a) Cross-section of Pt-10 wt% Rh wire Sample 1: Vickers hardness $HV0_{0.1}$ = 92 ± 4 (optical microscope after polishing, ×50, applied force: 0.1 N); (b) cross-section of Pt-10 wt% Rh wire Sample 2: Vickers hardness $HV0_{0.1}$ = 105 ± 4 (optical microscope after polishing, ×50, applied force: 0.1 N)

of the cross-sections of both wires are reported in **Figure 12**. In **Figure 11(b)** a coarser grain size is clearly observed for Sample 2. It is important to note that twins and low-angle grain boundaries can also be revealed by using the FIB source for surface etching, thus explaining why a larger number of grains are revealed by this method compared to the conventional chemical etching and optical microscopy. The difference in observed grains was resolved with the FIB, which showed that the large grains of Sample 2 are composed of smaller subgrains.

Nanohardness section profiles (**Figure 13**) confirmed a higher hardness for Sample 2. Nevertheless, the observed differences are reduced in comparison with data from microhardness testing (performed at 100 gf): this suggests that some artefacts are present during microhardness testing, likely due to bending (or buckling) of the wires during indentation. For nanoindentation testing, the results reported in **Figure 13** correspond to a penetration depth of 300 nm (applied load of about 1 gf), to avoid any artefact due to buckling or bending of the wire. It is also worth noting that some variation of nanohardness is observed from one grain to another.

A grain boundary is clearly visible for both samples. In the case of Sample 2 the TEM lamella was likely created at a twin boundary, as clearly identifiable in **Figure 14**. Looking at **Figures 14(b)** and **14(d)**,

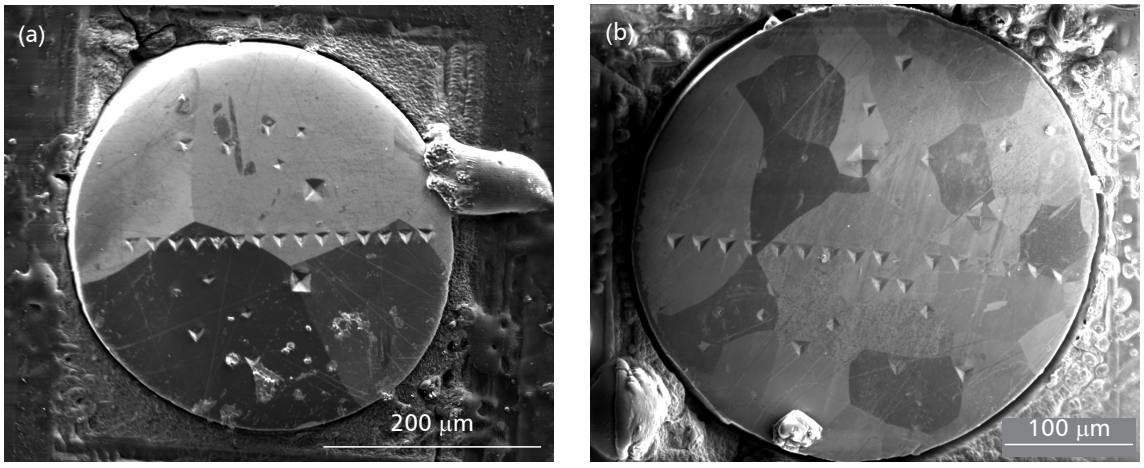

Fig. 12. Example of dualbeam analysis for: (a) Sample 1; and (b) Sample 2. Grain structure is clearly visible by using the ion source. The nanoindentation section profile is also clear in both cases. The TEM lamella was obtained at the sample edge corresponding to a grain boundary for each sample

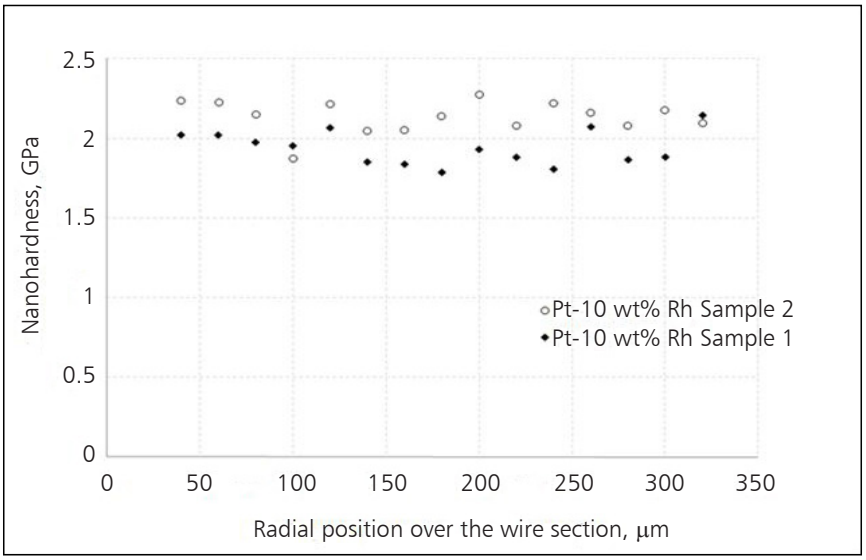

Fig. 13. Nanohardness cross-section profiles for both Pt-Rh wires under investigation (error bars have been removed for clarity)

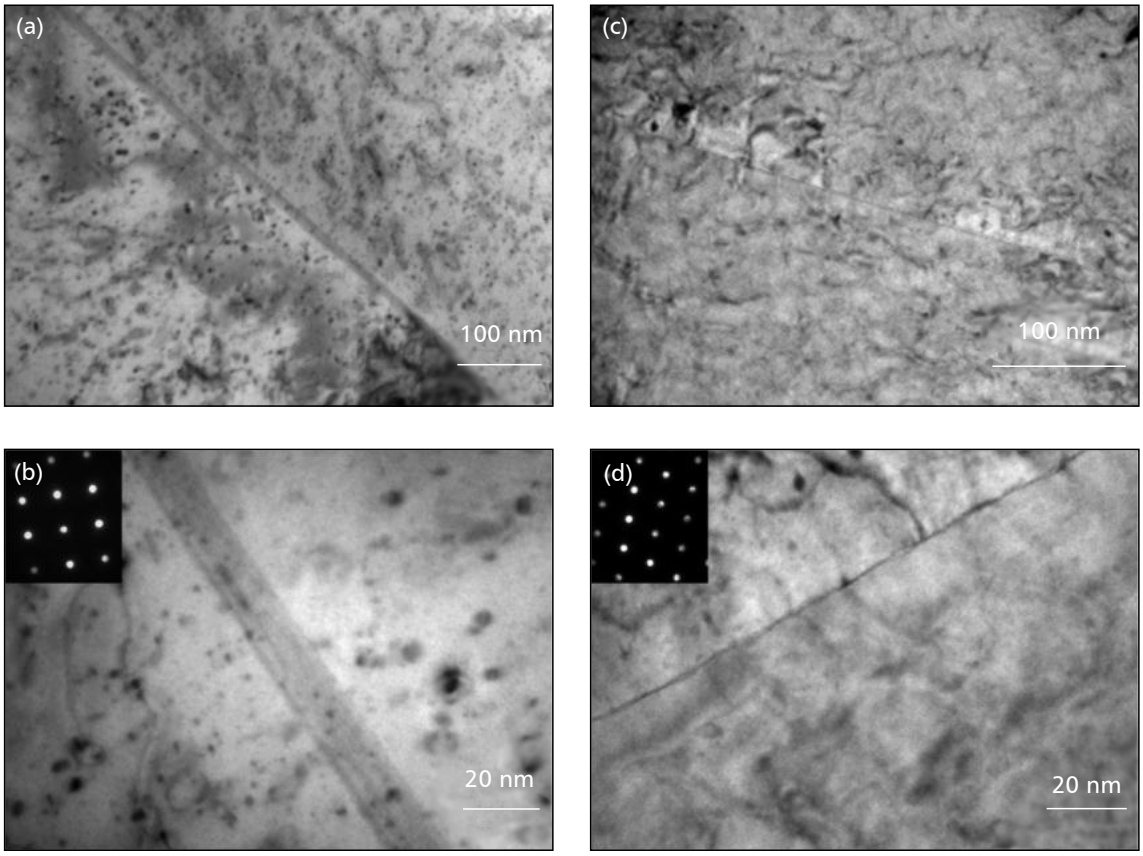

Fig. 14. TEM-SAED analysis on Sample 1: (a) TEM, 120 kV, ×140.000; (b) (TEM, 120 kV, ×660.000) – (TEM-SAED, 120 kV, Z = [100]); and Sample 2: (c) TEM, 120 kV, ×230.000; (d) (TEM, 120 kV, ×660.000) – (TEM-SAED, 120 kV, Z = [114])

significant microstructural differences can be identified between the two samples. In particular, Sample 1 is characterised by the presence of precipitates in the matrix (average diameter ~15 nm). In Sample 2, a different intragranular microstructure can be observed, mainly characterised by very fine precipitates dispersed in the matrix. The observed difference in micro- and nanoindentation hardness may therefore be due to differences of the intragrain phase distribution, which are likely strongly influenced by cooling rates during processing.

It is also worth noting that no differences in terms of crystal structure (SAED) and composition (EDS) were detected between the two samples, thus meaning that observed differences are essentially due to different (or not completely controlled) cooling rates during some of the processing steps.

To verify this latter hypothesis, both samples were subjected to a heat treatment at temperature of 450ºC for 1 h, followed by cooling in air. Results of the TEM analysis are reported in **Figure 15**, where a similar microstructure is observed in both cases. In this case, precipitates in the matrix of average diameter ~15 nm are also observed for Sample 2, thus confirming that the much finer subgrain microstructure that had been observed in the as-received Sample 2 was likely due to higher cooling rates during processing.

This example clearly explains how critical it is to properly control all parameters during the processing of these components. The use of high-resolution microscopy was in this case absolutely necessary to examine the actual correlations between the measured technological performance (for example, indentation hardness), the actual microstructural features of samples and the main process parameters.

4. Conclusions

This paper presents the application of high resolution, multitechnique and multiscale procedures to the nanomechanical characterisation of materials.

It was observed that a comprehensive characterisation of complex alloys can be achieved

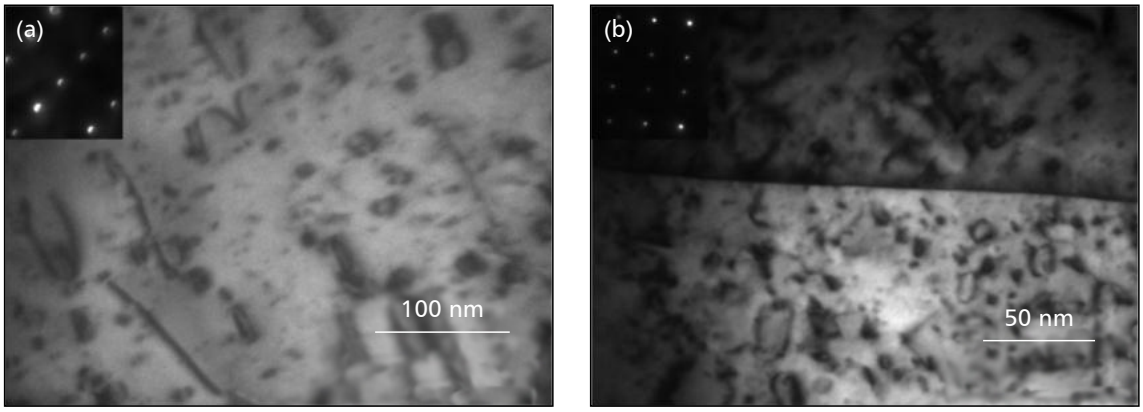

Fig. 15. (a) Sample 1 after heat treatment at 450°C for 1 h (TEM, 120 kV, ×230.000); (b) Sample 2 after heat treatment at 450°C for 1 h (TEM, 120 kV, ×380.000) – (Z = [100])

by the combination and synergic use of micro- and nanohardness testing and dualbeam-TEM techniques. Two case studies were reported relating to the nanomechanical and microstructural characterisation of an order hardened Pt-Cu alloy and a Pt-Rh wire alloy. In particular, the analysed case studies showed that nanoindentation testing can give valuable information on the level of microstructural changes as a consequence of phase transition and intragrain microstructure. The use of dualbeam-TEM combination technique may finally help to understand how and why microstructural changes due to heat treatment affect the mechanical properties of materials.

In the first case it was shown how the order-disorder transition in Pt-Cu alloys can be evaluated by indentation testing and that the analysis of hardness depth profiles can be extremely useful in suggesting the mechanisms of phase transition, which were later proved using high resolution microscopy, demonstrating that the order-disorder transition happens at a subgrain level only in previously cold worked alloy.

In the second case the use of FIB showed that the results from optical imaging of the grains were misleading, as were those from the microhardness test, because they did not give correct information of the real grain structure and the actual nanomechanical properties of the Pt-Rh wires. High resolution TEM imaging pointed to a likely mechanism (differences in nanoprecipitates) explaining the differences in hardness of the grains. With this work the existence of a miscibility gap and the absence of oxidation have been clearly shown, clarifying a point of contention between researchers in the field.

Such results clearly show how nanomechanical testing in combination with high resolution microscopy can be usefully applied to the characterisation of nanostructured systems for functional (or non-mechanical) application and how they can be a powerful tool for process optimisation and/or prediction of in-service behaviour.

Acknowledgments

This paper is dedicated to the memory of our wonderful friend and colleague, Dr Paolo Battaini, who recently passed away. The authors acknowledge the assistance of Daniele De Felicis during dualbeam characterisation activities, carried out at the "Interdepartmental Laboratory of Electron Microscopy" (LIME), University ROMA TRE, Rome, Italy, http://www.lime.uniroma3.it.

References

1 P. H. Mayrhofer, C. Mitterer, L. Hultman and H. Clemens, *Progr. Mater. Sci.*, 2006, **51**, (8), 1032

2 S. Zhang, D. Sun, Y. Fu and H. Du, *Surf. Coat. Technol.*, 2003, **167**, (2–3), 113

3 M.W. Phaneuf, *Micron*, 1999, **30**, (3), 277

4 "Introduction to Focused Ion Beams – Instrumentation, Theory, Techniques and Practice", 2nd Edn, eds. L. A. Giannuzzi and F. A. Stevie, Springer Science+Business Media, New York, USA, 2005

5 L. A. Giannuzzi and F. A. Stevie, *Micron*, 1999, **30**, (3), 197

6 W. C. Oliver and G. M. Pharr, *J. Mater. Res.*, 1992, **7**, (6), 1564

7 W. C. Oliver and G. M. Pharr, *J. Mater. Res.*, 2004, **19**, (1), 3

8 A. Bolshakov and G. M. Pharr, *J. Mater. Res.*, 1998, **13**, (4), 1049

9 S. J. Bull, *J. Phys. D: Appl. Phys.*, 2005, **38**, (24), R393

10 W. D. Nix and H. Gao, *J. Mech. Phys. Solids*, 1998, **46**, (3), 411

11 M. D. Uchic, D. M. Dimiduk, J. N. Florando and W. D. Nix, *Science*, 2004, **305**, (5686), 986

12 H. Bei, S. Shim, M. K. Miller, G. M. Pharr and E. P. George, *Appl. Phys. Lett.*, 2007, **91**, (11), 111915

13 A. M. Korsunsky, M. Sebastiani and E. Bemporad, *Mater. Lett.*, 2009, **63**, (22), 1961

14 C. Mshumi and C. Lang, *Platinum Metals Rev.*, 2007, **51**, (2), 78

15 M. Carelse and C. I. Lang, *Scripta Mater.*, 2006, **54**, (7), 1311

16 ASTM Standard E384, 'Standard Test Method for Knoop and Vickers Hardness of Materials', ASTM International, West Conshohocken, PA, 2011

17 D. Tabor, "The Hardness of Metals", Oxford University Press, New York, USA, 1951

18 ISO 14577-1/2:2002 'Metallic materials – Instrumented indentation test for hardness and materials parameters – Part 1: Test method' and 'Part 2: Verification and calibration of testing machines'

19 K. T. Jacob, S. Priya and Y. Waseda, *Metall. Mater. Trans. A*, 1998, **29**, (6), 1545

20 Z. M. Rdzawski and J. P. Stobrawa, *J. Mater. Process. Technol.*, 2004, **153–154**, 681

21 R. Wilkinson, *Platinum Metals Rev.*, 2004, **48**, (2), 88

22 R. Wilkinson, *Platinum Metals Rev.*, 2004, **48**, (3), 145

23 R. Wilkinson, *Platinum Metals Rev.*, 2005, **49**, (1), 60

24 R. Wilkinson, *Platinum Metals Rev.*, 2005, **49**, (2), 108

The Authors

Marco Sebastiani, PhD, is an Assistant Professor of Materials Science at the University of Rome "Roma Tre". His research is focused on surface engineering, micron-scale residual stress analysis and nanomechanical testing of thin films and nanostructured materials. He is the author of more than 40 papers in peer reviewed international journals.

Marco Renzelli received his Msc in Physics in 2010 at La Sapienza University of Rome. In January 2012 he started his PhD in Engineering at the University of Rome "Roma Tre". His interests lie in advanced materials production and characterisation, surface engineering, PVD technologies, focused ion beam microscopy and nanomechanical characterisation.

Paolo Battaini held a degree in nuclear engineering, had been a consulting engineer with 8853 SpA, and was a Professor of Precious Metal Working Technologies at Milano Bicocca University, Italy, from 2003 to 2011. He has been a recipient of the Santa Fe Symposium Research and Ambassador Award. He died on 27th September 2013.

Edoardo Bemporad is a nuclear engineer and holds a PhD in Materials Engineering. He is a full Professor of Materials Science and Technology at the University of Rome "Roma Tre". He is the author of more than 300 papers published in international and national journals, and his interests lie in structured and nanostructured coatings, especially for wear resistance, corrosion resistance and high temperature oxidation.

